Fused filament fabrication of polypropylene: Influence of the bead temperature on adhesion and porosity

Sébastien Charlon, Julien Le Boterff, Jérémie Soulestin

Version of Record: https://www.sciencedirect.com/science/article/pii/S2214860421000038
Manuscript_61d3dfa13c866c4e4ca883a43009517e

~~How to promote adhesion between polypropylene beads produced by molten polymer deposition additive manufacturing~~

Fused filament fabrication of polypropylene: influence of the bead temperature on adhesion and porosity

Sébastien CHARLON[1]*, Julien LE BORTERFF[1], Jérémie SOULESTIN[1]

1 IMT Lille Douai, Ecole nationale supérieure Mines-Télécom Lille Douai, Materials & Processes Centre, Cité scientifique, Villeneuve d'Ascq Cedex, France

*Corresponding author: sebastien.charlon@imt-lille-douai.fr

Abstract

~~The mechanical properties of the parts produced using fused filament fabrication (FFF) strongly depend on the adhesion strength between beads (F_A), which depends on process parameters. The aim of this work is to determine the influence of the manufacturing chamber temperature and nozzle temperature on the F_A between adjacent beads constituting two overlayed layers. Uniaxial tensile tests based on a Mode III fracture experiment associated with SEM observations allowed quantifying the influence of process parameters on F_A in parts made of polypropylene (PP). An increase in the manufacturing chamber temperature from 80 to 100°C causes a weak increase in F_A, while an increase in the nozzle temperature from 170 to 180°C causes a 145% F_A increase.~~

The mechanical properties of the parts produced using fused filament fabrication (FFF) strongly depend on the adhesion strength between beads (F_A), which substantially depends on the temperature of the polypropylene (PP) beads during their deposition. In this work, the temperature of the beads was controlled through the adjustment of the nozzle temperature (Tn) and the manufacturing chamber temperature (Tch) in order to control respectively the PP temperature at the nozzle end and the cooling of the PP beads after their deposition. SEM observations revealed an improvement of the coalescence between overlayed beads of different layers and between adjacent beads in the same layer with the increase in Tn. The increase of Tch promotes mainly the coalescence between adjacent beads within the layer. These observations were confronted with uniaxial tensile tests based on a Mode III fracture experiment allowed quantifying the influence of Tn and Tch on the adhesion strength between overlayed beads of different layers. Results reveals a weak increase in F_A caused by the increase in the manufacturing chamber temperature from 80 to 100°C, while an increase in the nozzle temperature from 170 to 180°C causes a 145% F_A increase. In the same time, this decrease in the manufacturing chamber temperature causes an important increase in porosity and a substantial decrease in the adhesion strength between layers.

Keywords: additive manufacturing, polymer, bead adhesion, structure, porosity

1. Introduction

Industrial interest in fused filament fabrication (FFF) has been growing because the process can manufacture parts with relatively little time, money and effort. Many parts can be produced using FFF,

such as functionalized, personalized, and/or lightened objects, prototypes, proofs of concept, or end-use products. These parts can be used in a wide range of applications, such as the transportation industry, sports, or education [1, 2].

Nevertheless, FFF seems to be less efficient than common processes, such as injection moulding, for manufacturing parts with strong mechanical properties [2, 3]. For example, manufacturing a part using FFF instead of injection moulding causes a decrease in tensile strength at break of approximately 12% in the case of acrylonitrile butadiene styrene (ABS) [4] and approximately 60% in the case of polyether-ether-ketone (PEEK) [5]. In the same way, the impact strength of ABS parts is 80% lower than that of injected parts [4–8]. The mechanical properties of a part strongly depend on its structure, particularly its intrinsic porosity. An injected part is fully dense because of high pressure applied to molten material during the process, while a high level of porosity is often observed in FFF parts [3,9,10]. The FFF process consists of stacking polymer layers to form a 3D part previously designed with computer aided design (CAD) software. Each layer is composed of polymer beads deposited in the molten state beside the other beads. The cylindrical geometry of the beads causes the formation of pores inside the FFF part. [11]. Several authors tried to reduce the porosity of FFF parts with optimization of process parameters [10,12–14]. Gajdoš et al. [15] revealed a 2% porosity decrease in ABS parts using a 5°C increase in chamber temperature, while Zekavat et al [12] showed a 10% decrease in porosity by increasing the nozzle temperature from 180°C to 260°C to manufacture PLA parts. Increasing temperatures (nozzle and chamber) promotes polymer chain diffusion between beads and thus their coalescence, which is a fundamental phenomenon affecting the residual porosity in the part.

Mechanical properties of FFF parts are strongly governed not only by the intrinsic porosity but also by the adhesion strength between beads (F_A). In the literature, authors have shown the dependence of F_A on process parameters, such as the bead deposition strategy or nozzle temperature [4,16,17]. Davis et al. [17] measured an F_A between two ABS beads at 5 $N.mm^{-1}$ with a nozzle temperature of 210°C, and it was found to be equal to 25 $N.mm^{-1}$ with a nozzle temperature of 250°C. At a low nozzle temperature, polymer chains do not have sufficient mobility to diffuse effectively across the interface, leading to a form of low F_A. As the nozzle temperature increases, reptation and entanglement of polymer chains are promoted across the interface because of a chain diffusion increase. As a result, the F_A is strongly increased. Yin et al. [18] also studied the influence of process parameters (temperatures and velocity) on F_A for two polymers (thermoplastic polyurethane (TPU) and ABS). Increasing the building velocity from 8 to 12 $mm.s^{-1}$ causes a 6% F_A increase, while increasing the temperature of the build plate from 30°C to 68°C causes an 88% F_A increase. With a high build plate temperature, the cooling of molten polymer is reduced, favouring coalescence. Promoting coalescence is a key point for optimizing F_A because it favours the diffusion of polymer chains and increases the contact surface between beads. Therefore, promoting coalescence is a key point for optimizing mechanical properties of FFF parts because it increases F_A and decreases the intrinsic porosity.

We believe that no work has studied F_A in an FFF part composed of polypropylene (PP), while production of PP parts using FFF has been generating industrial interest in many fields, such as automotive, aeronautics and medical applications [22–31]. Indeed, PP is highly competitive compared with other polymers because of its great advantages, such as a low density, high impact strength, chemical and thermal resistances, diversity, recyclability and low cost [25]. Moreover, the literature has clearly revealed the importance of the nozzle temperature on F_A, but the influence of the manufacturing chamber temperature is not well understood. The objective of this work is therefore to study the influence of the nozzle temperature and manufacturing chamber temperature on F_A in parts

made of PP produced with a manufacturing machine equipped with a thermally regulated manufacturing chamber.

2. Experimental section

2.1. Materials

In this study, a polypropylene, grade MR10MM0 (Total, France) was used. The chosen grade is characterized by a density of 0.902 g.cm^{-3} and a melting temperature of 131°C.

2.2. Process

Each sample studied in this work was made using a Freeformer additive manufacturing machine (Arburg, Germany) equipped with a thermally regulated manufacturing chamber. The machine combines injection and FFF technologies. Indeed, polymer pellets are loaded into a hopper that feeds a plasticization unit comprised of an injection screw placed in a heated barrel. Hence, polymer pellets are melted, sheared and carried to a discharge unit. The discharge unit is comprised of a high-frequency piezo actuator (145 Hz) coupled with a needle at the nozzle end (Figure 1a). Theoretically, the high frequency of the opening/closing cycle of the nozzle end causes a discharge of discontinuous droplets of molten polymer. In practice, the nozzle is never completely closed because of molten polymer viscoelasticity and the high frequency of the piezo actuator. Hence, deposited droplets are connected (Figure 1b) so that deposited material can be described as a bead, similar to what is observed for the FFF process. The droplet volume is controlled by pressure applied to the molten polymer by the screw and by a high frequency opening/closing system. In this study, the pressure and frequency were kept constant to maintain a constant droplet volume whatever the process parameters. Beads are deposited onto a build plate moving in the x- and y-directions. Once the current layer is finished, the build plate is lowered (z-direction) and the next layer begins.

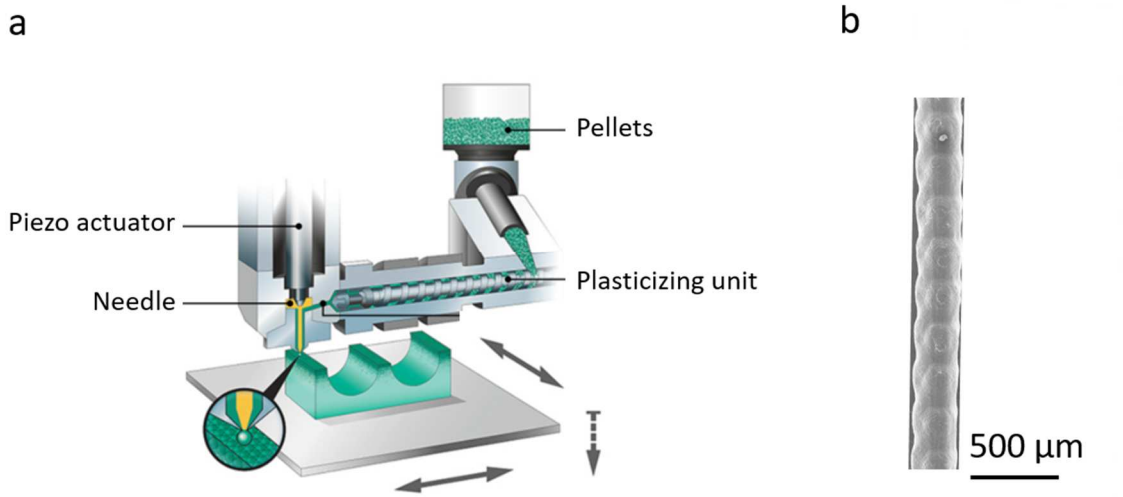

Figure 1: a) Scheme of a plasticization unit in the Freeformer machine [32]. *b) SEM images of beads produced by the Freeformer machine*

2.3. Sample preparation

~~Samples of size 150 × 9 × 0.66 mm manufactured by a Freeformer machine have a 22 layer height and 2 bead width (Figure 2).~~

The dimensions of the rectangular parallelepiped CAD model used to manufacture the samples are x=0.66 * y=150 * z= 6 mm (Figure 2a). The samples are constituted by 2 beads in x directions and by 22 layers in z directions. The layer thickness was fixed at 0.27 mm. Three nozzle temperatures

(Tn=170°C, Tn=175°C and Tn=180°C) and two manufacturing chamber temperatures (Tch=80°C and Tch=100°C) were tested. ~~The slicing distance corresponding to the nozzle end/build plate distance was fixed at 0.27 mm.~~

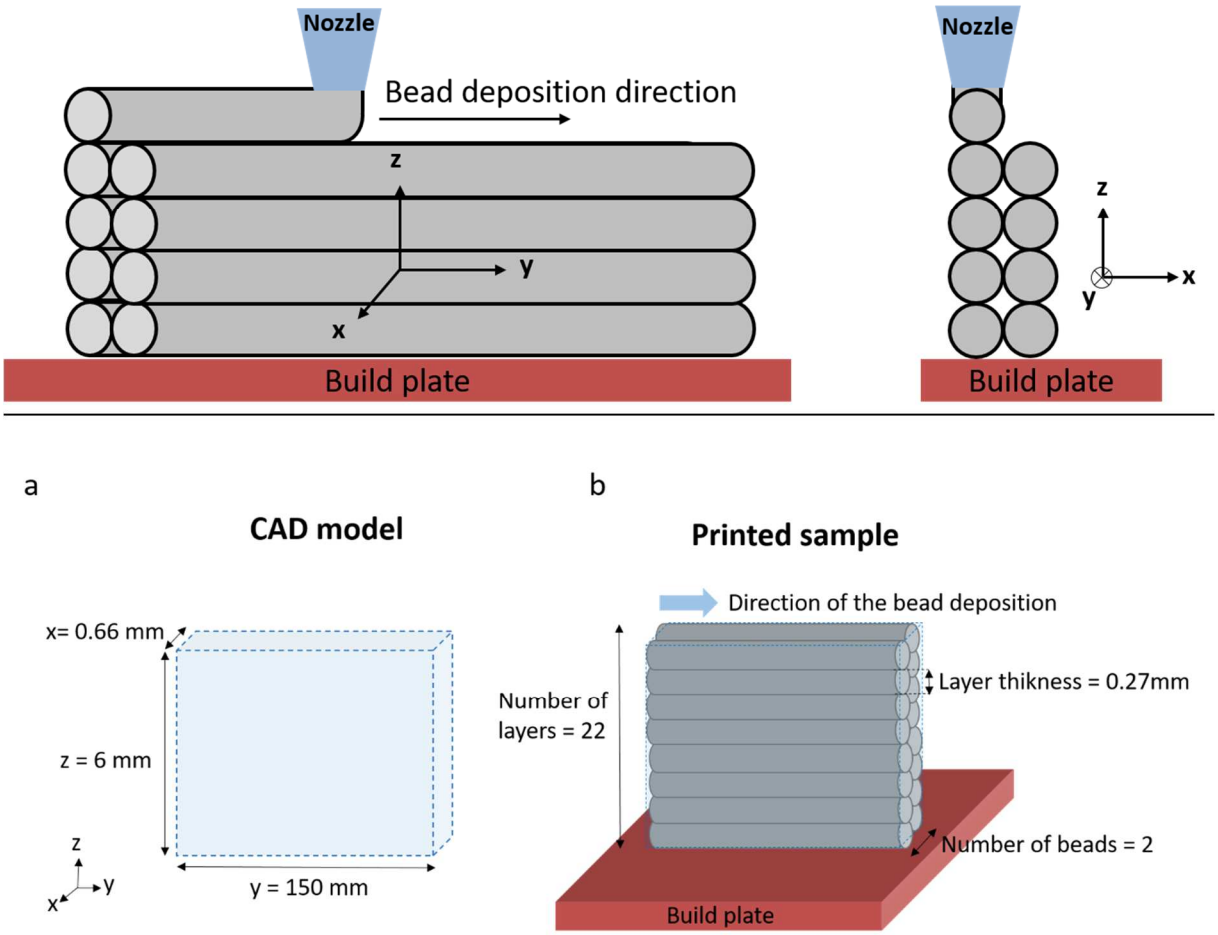

Figure 2: Schematic representations of sample bead deposition

2.4. Measurement of the inter-bead adhesion strength

The inter-bead adhesion strength was determined using the Mode III "trouser tear" fracture experiment (Figure 3b) according to ASTM D1938 standard [33] (Figure 3c). The Mode III fracture is particularly adapted to measure F_A because it generates local tearing adapted to thin and flat samples, such as pressed sheets or films.

The previously manufactured samples were precisely notched under a microscope between the 11th and 12th layers (Figure 3a) corresponding to the half-height of the sample. Sample part B was then clamped in the bottom pulling jaw of a uniaxial tensile test machine Lloyd LR50K, while sample part A was clamped in the top pulling jaw (Figure 3b).

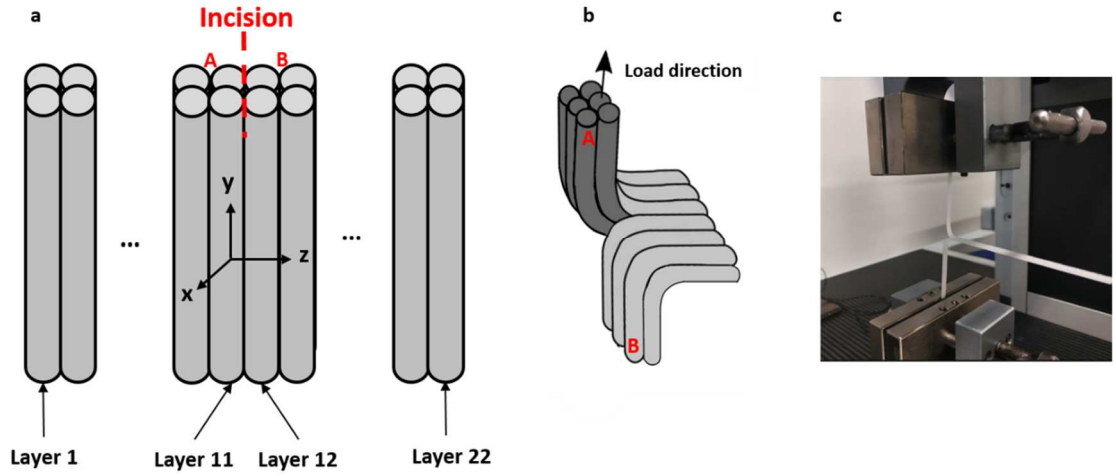

Figure 3: Protocol used to measure the adhesion strength. a) Location of the incision performed between the 11th and 12th layers. b) Typical testing configuration of a sample during a measurement. c) Photograph of tests performed with a uniaxial tensile test machine.

The adhesion strength, corresponding in these conditions to the strength needed to delaminate two adjacent layers, was measured with a 1 mm.s^{-1} displacement speed at a 100 mm sample distance with a 100 N load cell. The sample untorn part remained orthogonal to the load direction during all tests, without any torsion or rotation (Figure 3c). The adhesion strength between beads (F_A) was considered the average strength during the steady state crack propagation (Figure 4a). The measured F_A was normalized either by the sample thickness (t_S) or by the inter-bead contact length (t_{cl}) (Figure 4b). The resulting normalized adhesion strengths were respectively denoted σ_N and σ_A (Equations 1 and 2).

$$\sigma_N = \frac{F_A}{t_S} \quad Equation\ 1 \qquad\qquad \sigma_A = \frac{F_A}{t_{cl}} \quad Equation\ 2$$

The adhesion strengths were measured in 6 reproducible tests (Figure 4a).

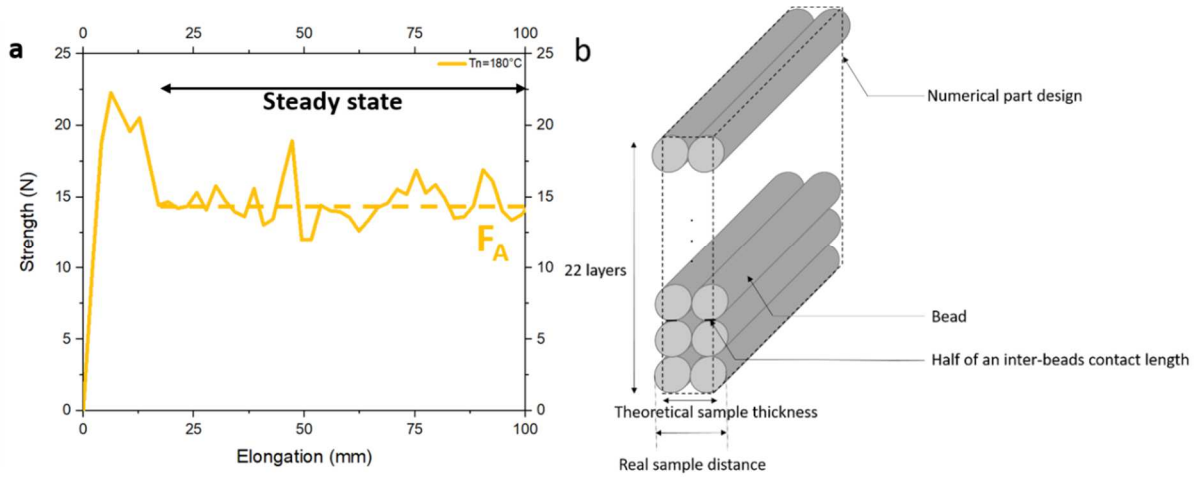

Figure 4: a) Typical curve obtained during an inter-bead adhesion strength measurement and b) a schematic representation of the sample structure.

2.5. Measurements of the sample thickness and distance between beads (contact length)

Samples were first cryofracturized under liquid nitrogen following the XZ plane (Figure 3a). A cross section of the samples was gold metallized using an Agar Scientific sputter coater B7340 (United Kingdom) for 30 s with a 30 mA intensity and a vacuum lower than 0.03 mbar. The sample cross section was observed using a scanning electron microscope (SEM) JEOL NeoScope II JCM-6000 PLUS (Japan). The contact length and sample thickness were measured on resulting SEM images using ImageJ software. The average contact length and sample thickness were calculated from at least 5 measurements performed on 3 samples per process condition.

3. Results and discussion

3.1. Influence of the process parameters on the sample structure

The variation in the nozzle temperature (Tn) and manufacturing chamber temperature (Tch) is supposed to modify the structure of FFF parts. Therefore, the cross section of each manufacturing sample was observed using an SEM (Figure 5).

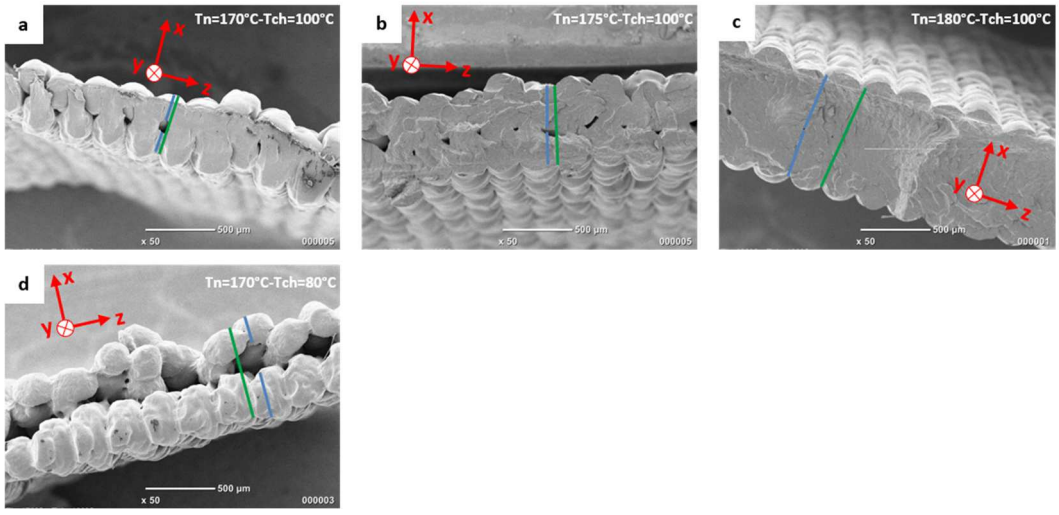

Figure 5: SEM images of sample cross sections manufactured with several process parameters (blue lines show examples of contact length and green lines show examples of sample thickness): a) Tn=170°C, Tch=100°C, b) Tn=175°C, Tch=100°C, c) Tn=180°C, Tch=100°C, and d) Tn=170°C, Tch=80°C.

The sample thickness (t_S) and contact length (t_{cl}) were determined on SEM images and plotted as a function of the nozzle temperature and manufacturing chamber temperature, as shown on Figure 6. A comparison between the sample thickness and contact length is an indicator of sample porosity. A contact length smaller than the sample thickness is associated with a porous sample, while an equality between the two distances indicates a fully dense sample (Figure 5b).

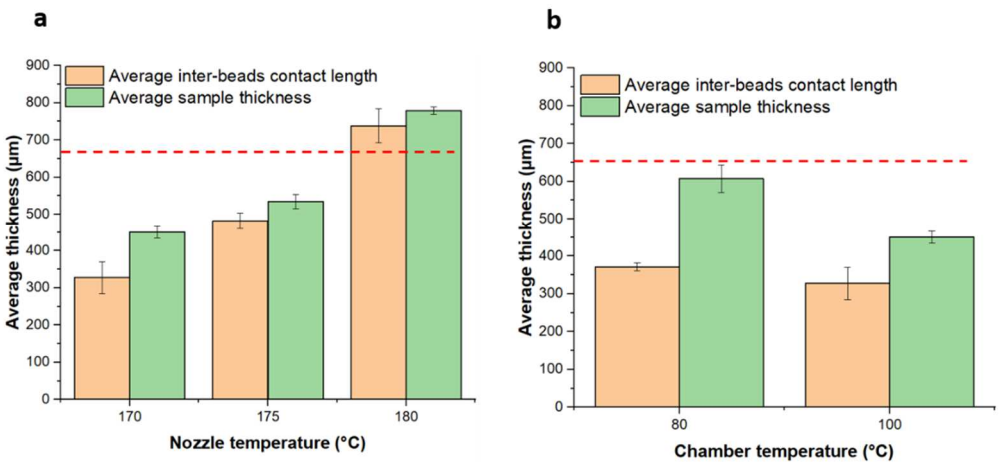

Figure 6: Bar plots of the contact length and sample thickness against the nozzle temperature (a) and manufacturing chamber temperature (b). The red dashed line represents the sample thickness (660 µm) as set in the software.

The SEM images and contact lengths shorter than the sample thickness for each manufactured sample reveal a high intrinsic porosity level in manufactured samples. This result is in good agreement with the literature in the case of ABS and PLA parts made using FFF [10,12,16,17,34–36].

Figure 5 and Figure 6 also reveal the strong effects of the nozzle and manufacturing chamber temperatures on sample structure. Increasing the manufacturing chamber temperature from Tch=80°C to Tch=100°C causes a drastic reduction in the sample porosity (Figure 5), a decrease in sample thickness and an increase in contact length. Indeed, molten PP beads were cooled at a lower rate from the nozzle temperature (Tn=170°C) to the manufacturing chamber temperature Tch=100°C than to Tch=80°C. The lower cooling rate promotes coalescence between beads and results in a higher contact length. It also decreases the sample thickness and porosity.

Increasing the nozzle temperature from 170°C to 180°C causes a significant reduction in sample porosity (Figure 5) and an increase in sample thickness and contact length (Figure 6). Increasing the nozzle temperature increases the molten PP temperature and therefore decreases its viscosity. The mobility of PP polymer chains is therefore increased, promoting coalescence. Moreover, molten PP beads fit the surface roughness of the previously deposited layer, leading to a reduction in sample porosity. However, decreasing the PP viscosity also favours wall creep during the fabrication of the layer. PP beads spread and flatten onto the previously deposited layer until their solidification, leading to an increase in sample thickness.

3.2. Influence of the nozzle temperature on adhesion strength

The influence of the nozzle temperature on adhesion strength was studied using a uniaxial tensile test machine. The resulting curves illustrating traction strength versus elongation displacement for three nozzle temperatures and one constant manufacturing chamber temperature (Tch=100°C) are plotted in Figure 7.

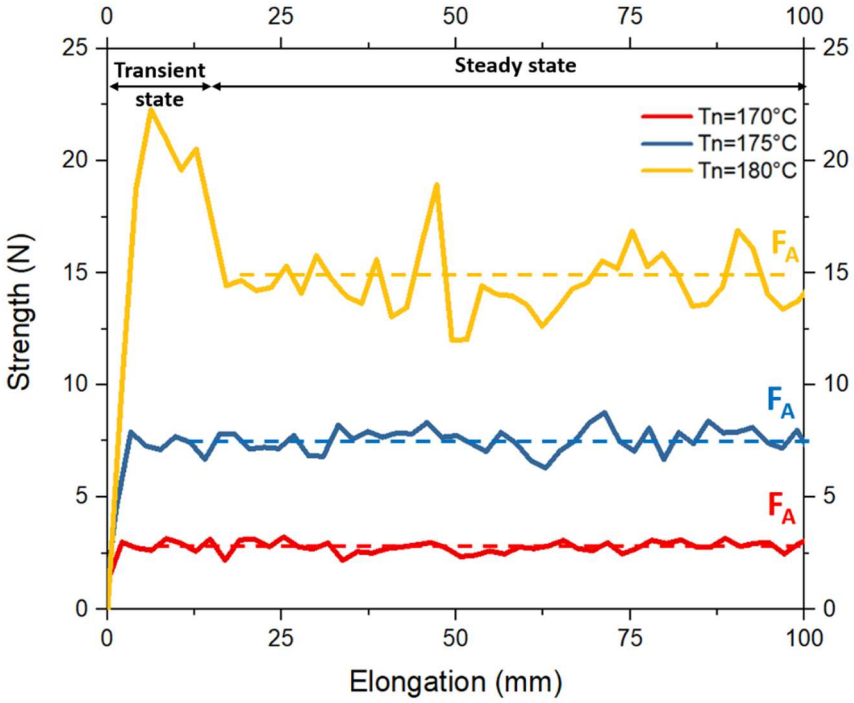

Figure 7: Curves illustrating traction strength versus elongation for samples manufactured with three nozzle temperatures (Tn=170, 175 and 180°C) and a constant manufacturing chamber temperature (Tch=100°C). Dashed lines represent the average inter-bead adhesion strength in samples.

Each curve shows two different parts: a transient and a stationary state. The stabilization of the strength needed to propagate the tearing is associated with the transient state, while the stabilized strength needed to propagate the tearing is associated with the steady state. Because the sample thickness and contact length were affected by the nozzle temperature, adhesion strengths normalized by the sample thickness (σ_N) and by the contact length (σ_A) were calculated from the steady state and plotted in Figure 8.

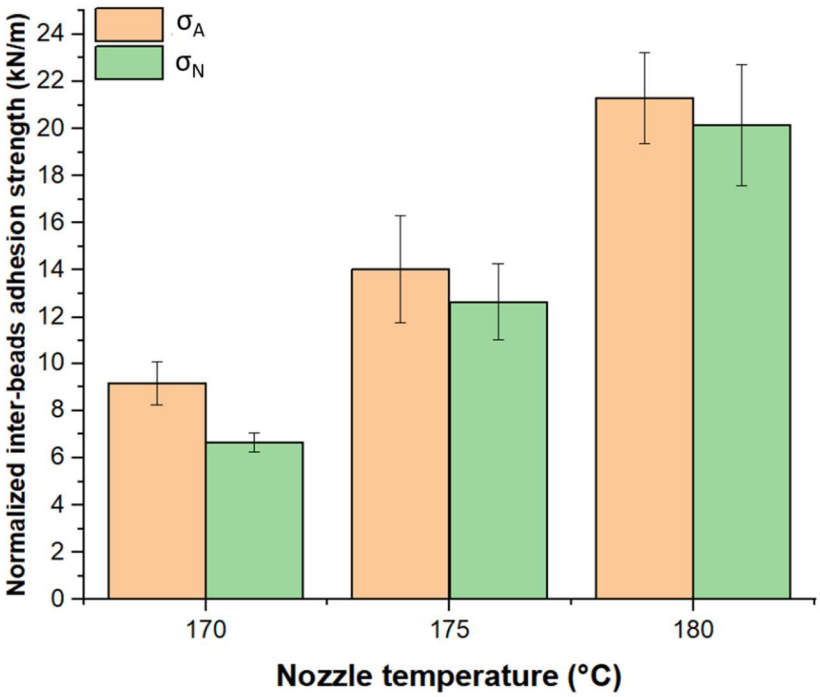

Figure 8: *Adhesion strength normalized by contact length (σ_A) and sample thickness (σ_N) as a function of nozzle temperature.*

The adhesion strength normalized by sample thickness (σ_N) corresponds to the real strength needed to separate two adjacent layers, while the adhesion strength normalized by contact length (σ_A) corresponds to the strength needed to separate two adjacent layers of a supposedly fully dense sample. As expected, σ_A is higher than σ_N because each studied sample is porous. The gap between σ_A and σ_N decreases with increasing nozzle temperature because of a part porosity decrease. Indeed, increasing the nozzle temperature decreases the PP viscosity, which promotes coalescence and decreases porosity. (Figure 5a, b and c).

Figure 8 also reveals the strong dependence of the normalized adhesion strength on nozzle temperature: a higher nozzle temperature causes a higher adhesion strength. For a high nozzle temperature, the viscosity of molten PP is low (mobility of polymer chains is high), and the kinetics of coalescence is therefore fast. As a consequence, a large interphase must be created between beads before their solidification, which promotes the adhesion strength. In contrast, at lower nozzle temperatures, the viscosity of molten PP is high (mobility of polymer chains is low), and the kinetics of coalescence is therefore slow. As a consequence, a low interphase between adjacent beads must be created before their solidification, which decreases the adhesion strength.

3.3. Influence of the chamber temperature on the adhesion strength

The influence of the chamber temperature on the adhesion strength was also studied using a uniaxial tensile test machine. The resulting curves illustrating tensile strength versus elongation for two manufacturing chamber temperatures (Tch=80°C and Tch=100°C) and a constant nozzle temperature (Tn=170°C) are plotted in Figure 9.

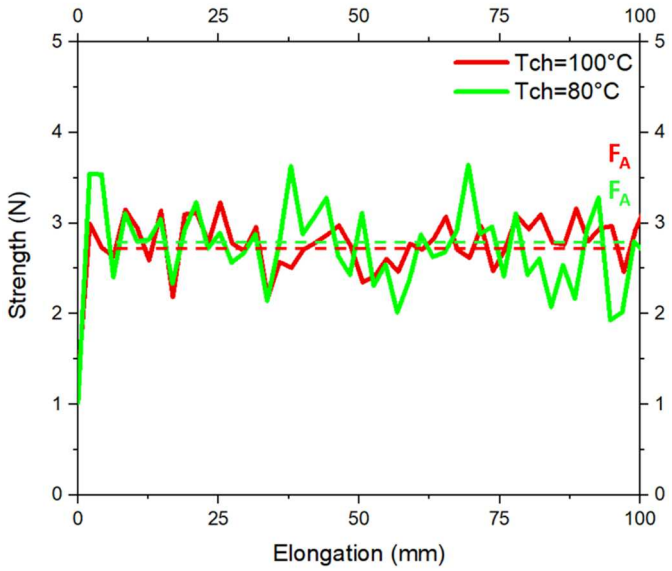

Figure 9: Curves illustrating traction strength versus elongation obtained on samples manufactured with two manufacturing chamber temperatures (Tch=80°C and Tch=100°C) and a constant nozzle temperature (Tn=170°C). Dashed lines represent the average adhesion strength in the samples.

Because the thickness and contact length were affected by the nozzle temperature, the adhesion strengths normalized by sample thickness (σ_N) and contact length (σ_A) were calculated from the steady state and plotted in Figure 10.

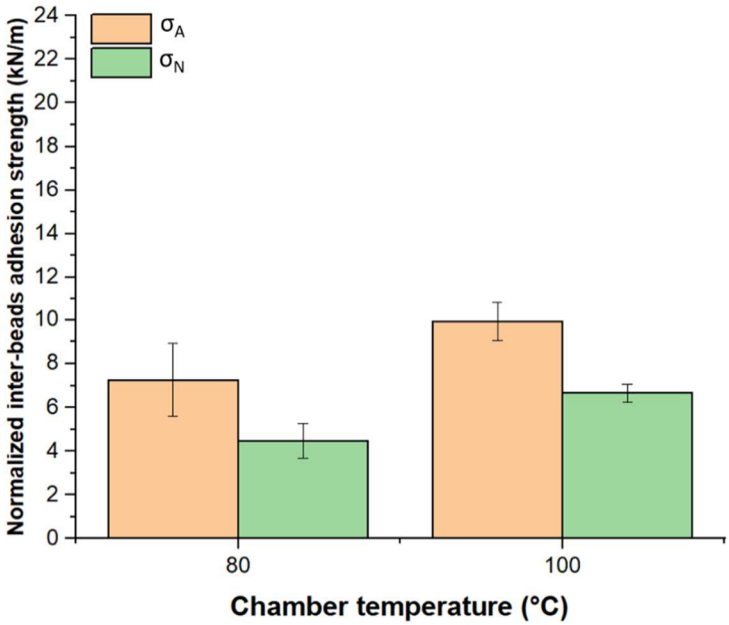

Figure 10: Adhesion strength normalized by the contact length (σ_A) and sample thickness (σ_N) as a function of the manufacturing chamber temperature.

Figure 9 reveals a weak dependence of the adhesion strength on the manufacturing chamber temperature. Increasing the manufacturing chamber temperature slightly increases the adhesion strength. In this work, the adhesion strength was measured in the XZ plane (Figure 3). In other words, the adhesion strength was measured between overlayed beads constituting two layers. However,

Figure 9 does not provide any information on the adhesion strength between two adjacent beads in the same layer (XY plane).

3.4. Comparison of the influence of the nozzle and chamber temperatures on the adhesion strength

The nozzle temperature and manufacturing chamber temperature affect the structure of the part differently. According to the SEM images (Figure 5), the nozzle temperature greatly affects the contact length between overlayed beads of different layers (XZ plane) and adjacent beads in the same layer (XY plane). As explained in section 4.2 (Influence of the nozzle temperature on the adhesion strength), an increase in the nozzle temperature causes a cascade of events: a decrease in molten polymer viscosity, an increase in the kinetics of coalescence, an increase in the contact length, a decrease in the porosity and finally an increase in the adhesion strength. Because molten beads are deposited next to adjacent beads (XY plane) and overlayed on the previous layer (XZ plane), this cascade of events occurs in the XY (same layer) and XZ planes (different layers). Moreover, increasing the molten polymer temperature must favour the surface melt of the adjacent and overlayed beads, promoting coalescence and therefore increasing the adhesion strength in the XY and XZ planes (Figure 11).

The manufacturing chamber temperature substantially influences the contact length between adjacent beads in the same layer (XY plane). Indeed, the chamber temperature affects the cooling rate of the deposited beads. At a higher chamber temperature, a lower cooling rate for the beads delays the solidification of the polymer, leaving more time for coalescence. Considering the deposition pathway (Figure 11), a molten bead is deposited next to a "warm" one (same layer) and on a "cold" one (previous layer). Therefore, increasing the temperature of the manufacturing chamber promotes coalescence between two adjacent beads in the same layer. However, it does not substantially affect coalescence between the overlayed beads of consecutive layers. These results are in good agreement with the adhesion strength measured between adjacent layers (Figure 8 and Figure 10).

A schematic representation of the influence of the nozzle and chamber temperatures is proposed in Figure 11.

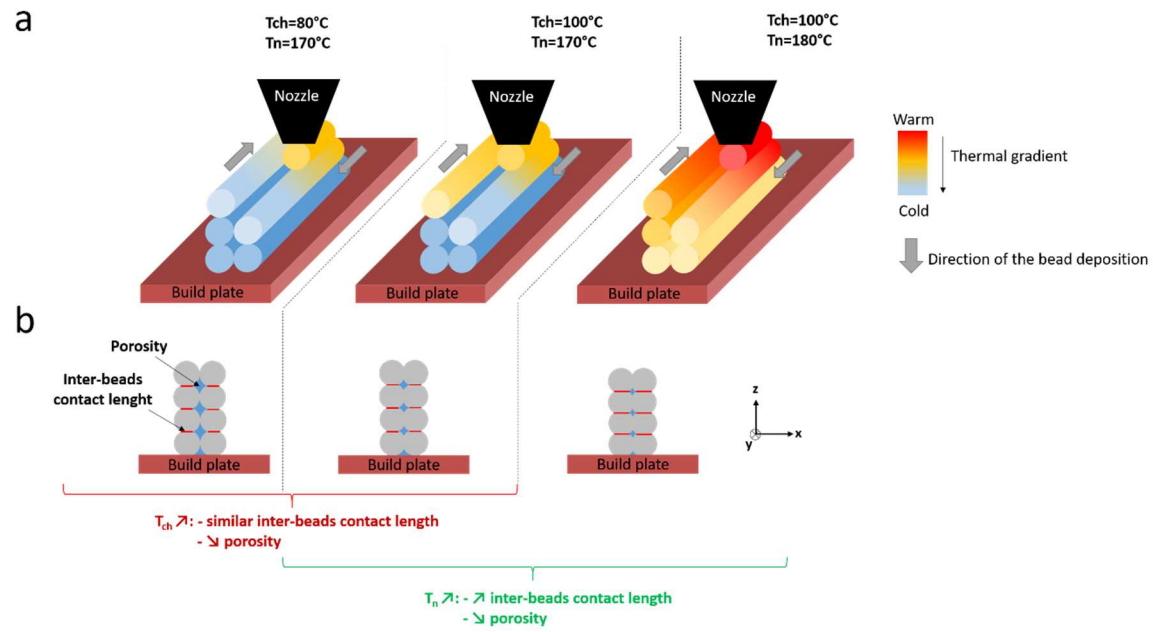

Figure 11: Schematic representation of the influence of the nozzle and manufacturing chamber temperatures on the bead temperature (a) and on the contact length in the XY plane (b).

Unfortunately, the protocol used in this study does not allow for measuring the adhesion strength between adjacent beads of the same layer (XY plane). Indeed, making the incision under the microscope between two adjacent beads constituting the same layer is very difficult and cannot provide any reproducible results using the type of sample manufactured in this work. Samples with a different geometry would have to be manufactured to study the adhesion strength between adjacent beads in the same layer.

4. Conclusion

The mechanical properties of the part produced by molten polymer deposition additive manufacturing strongly depend on its residual porosity and on the adhesion strength. In this work, the influence of nozzle temperature and manufacturing chamber temperature on the adhesion strength between PP beads constituting two overlayed layers was studied. Increasing the nozzle temperature causes a decrease in molten polymer viscosity, which favours coalescence, leading to an improvement in the contact between two overlayed beads of different layers. As a result, it greatly increases the adhesion strength between layers. Moreover, a higher nozzle temperature also increases the contact length between adjacent beads (same layer) because of the same phenomenon. Increasing the manufacturing chamber temperature has a slight effect on the adhesion strength between layers. Even if an increasing manufacturing chamber temperature causes a decrease in the cooling rate of the beads, considering the deposition pathway, beads are deposited on a “cold” layer, which negatively influences coalescence between overlayed beads. Considering a layer fabrication, beads are deposited next to “warm” adjacent beads (same layer), promoting coalescence. As a result, the contact length between two adjacent beads is increased, which must also increase the adhesion strength.

Thus, increasing the nozzle temperature must be recommended to substantially increase the part mechanical properties. However, special attention should be paid to creep phenomena and to polymer chains degradation associated with a too high nozzle temperature setting. The resulting tendencies shown in this work could be used for each molten polymer deposition additive manufacturing process (FFF, AFP, etc.) using any thermoplastic polymer. It also demonstrates that the use a thermo-regulated manufacturing chamber is essential for obtaining a high-quality part from semicrystalline polymers in general and PP in particular. Decreasing the manufacturing chamber temperature from 100°C to 80°C for PP causes an important increase in porosity and to a substantial decrease in the adhesion strength between layers. This study provides the first evidence of the necessity of using a high manufacturing chamber temperature to obtain high quality parts. An optimized manufacturing chamber temperature will depend on the polymers used. One can suppose that this temperature must be above the glass transition temperature for amorphous polymers and near the crystallization temperature for semicrystalline polymers.

Acknowledgement

The authors are greatly thankful to the region Haut de France for financial support.

References

[1] K. V. Wong, A. Hernandez, A Review of Additive Manufacturing, ISRN Mech. Eng. 2012 (2012) 1–10. doi:10.5402/2012/208760.

[2] M. Attaran, The rise of 3-D printing: The advantages of additive manufacturing over traditional manufacturing, Bus. Horiz. 60 (2017) 677–688. doi:10.1016/j.bushor.2017.05.011.

[3] L.E.J. Thomas-Seale, J.C. Kirkman-Brown, M.M. Attallah, D.M. Espino, D.E.T. Shepherd, The barriers to the progression of additive manufacture: Perspectives from UK industry, Int. J.

Prod. Econ. 198 (2018) 104–118. doi:10.1016/j.ijpe.2018.02.003.
[4] M. Dawoud, I. Taha, S.J. Ebeid, Mechanical behaviour of ABS: An experimental study using FFF and injection moulding techniques, J. Manuf. Process. 21 (2016) 39–45. doi:10.1016/j.jmapro.2015.11.002.
[5] W. Wu, P. Geng, G. Li, D. Zhao, H. Zhang, J. Zhao, Influence of Layer Thickness and Raster Angle on the Mechanical Properties of 3D-Printed PEEK and a Comparative Mechanical Study between PEEK and ABS, Materials (Basel). 8 (2015) 5834–5846. doi:10.3390/ma8095271.
[6] S. Ahn, M. Montero, D. Odell, S. Roundy, P.K. Wright, Anisotropic material properties of fused deposition modeling ABS, Rapid Prototyp. J. 8 (2002) 248–257. doi:10.1108/13552540210441166.
[7] G.D. Kim, Y.T. Oh, A benchmark study on rapid prototyping processes and machines: Quantitative comparisons of mechanical properties, accuracy, roughness, speed, and material cost, Proc. Inst. Mech. Eng. Part B J. Eng. Manuf. 222 (2008) 201–215. doi:10.1243/09544054JEM724.
[8] M. Montero, S. Roundy, D. Odell, S.-H. Ahn, P.K. Wright, Material Characterization of Fused Deposition Modeling (FFF) ABS by Designed Experiments, 2001. http://ode11.com/publications/sme_rp_2001.pdf (accessed March 4, 2019).
[9] W. Jo, O.-C. Kwon, M.-W. Moon, Investigation of influence of heat treatment on mechanical strength of FFF printed 3D objects, Rapid Prototyp. J. 24 (2018) 637–644. doi:10.1108/RPJ-06-2017-0131.
[10] K. Chin Ang, K. Fai Leong, C. Kai Chua, M. Chandrasekaran, Investigation of the mechanical properties and porosity relationships in fused deposition modelling-fabricated porous structures, Rapid Prototyp. J. 12 (2006) 100–105. doi:10.1108/13552540610652447.
[11] J. Gardan, Additive manufacturing technologies: state of the art and trends, Int. J. Prod. Res. 54 (2016) 3118–3132. doi:10.1080/00207543.2015.1115909.
[12] A.R. Zekavat, A. Jansson, J. Larsson, L. Pejryd, Investigating the effect of fabrication temperature on mechanical properties of fused deposition modeling parts using X-ray computed tomography, Int. J. Adv. Manuf. Technol. 100 (2019) 287–296. doi:10.1007/s00170-018-2664-8.
[13] O.S. Es-Said, J. Foyos, R. Noorani, M. Mendelson, R. Marloth, B.A. Pregger, Effect of Layer Orientation on Mechanical Properties of Rapid Prototyped Samples, Mater. Manuf. Process. 15 (2000) 107–122. doi:10.1080/10426910008912976.
[14] S. Ding, B. Zou, P. Wang, H. Ding, Effects of nozzle temperature and building orientation on mechanical properties and microstructure of PEEK and PEI printed by 3D-FFF, Polym. Test. 78 (2019) 105948. doi:10.1016/j.polymertesting.2019.105948.
[15] I. Gajdoš, J. Slota, Influence of printing conditions on structure in FFF prototypes | Utjecaj uvjeta tiskanja na strukturu FFF prototipova, Teh. Vjesn. 20 (2013) 231–236.
[16] C. Ziemian, M. Sharma, S. Ziemi, Anisotropic Mechanical Properties of ABS Parts Fabricated by Fused Deposition Modelling, in: Mech. Eng., InTech, 2012. doi:10.5772/34233.
[17] C.S. Davis, K.E. Hillgartner, S.H. Han, J.E. Seppala, Mechanical strength of welding zones produced by polymer extrusion additive manufacturing, Addit. Manuf. 16 (2017) 162–166. doi:10.1016/j.addma.2017.06.006.
[18] J. Yin, C. Lu, J. Fu, Y. Huang, Y. Zheng, Interfacial bonding during multi-material fused deposition modeling (FFF) process due to inter-molecular diffusion, Mater. Des. 150 (2018) 104–112. doi:10.1016/j.matdes.2018.04.029.
[19] A. Bellini, S. Güçeri, Mechanical characterization of parts fabricated using fused deposition modeling, Rapid Prototyp. J. 9 (2003) 252–264. doi:10.1108/13552540310489631.
[20] N. Hill, M. Haghi, Deposition direction-dependent failure criteria for fused deposition modeling polycarbonate, Rapid Prototyp. J. 20 (2014) 221–227. doi:10.1108/RPJ-04-2013-0039.
[21] A.R. Torrado Perez, D.A. Roberson, R.B. Wicker, Fracture Surface Analysis of 3D-Printed Tensile Specimens of Novel ABS-Based Materials, J. Fail. Anal. Prev. 14 (2014) 343–353. doi:10.1007/s11668-014-9803-9.
[22] O.S. Carneiro, A.F. Silva, R. Gomes, Fused deposition modeling with polypropylene, Mater. Des. 83 (2015) 768–776. doi:10.1016/j.matdes.2015.06.053.

[23] B. Kaynak, M. Spoerk, A. Shirole, W. Ziegler, J. Sapkota, Polypropylene/Cellulose Composites for Material Extrusion Additive Manufacturing, Macromol. Mater. Eng. 303 (2018) 1800037. doi:10.1002/mame.201800037.
[24] M. Spoerk, J. Sapkota, G. Weingrill, T. Fischinger, F. Arbeiter, C. Holzer, Shrinkage and Warpage Optimization of Expanded-Perlite-Filled Polypropylene Composites in Extrusion-Based Additive Manufacturing, Macromol. Mater. Eng. 302 (2017) 1700143. doi:10.1002/mame.201700143.
[25] M. Spoerk, J. Gonzalez-Gutierrez, C. Lichal, H. Cajner, G. Berger, S. Schuschnigg, L. Cardon, C. Holzer, Optimisation of the Adhesion of Polypropylene-Based Materials during Extrusion-Based Additive Manufacturing, Polymers (Basel). 10 (2018) 490. doi:10.3390/polym10050490.
[26] S. Hertle, M. Drexler, D. Drummer, Additive Manufacturing of Poly(propylene) by Means of Melt Extrusion, Macromol. Mater. Eng. 301 (2016) 1482–1493. doi:10.1002/mame.201600259.
[27] R. Jagenteufel, T. Hofstaetter, F. Kamleitner, D. B. Pedersen, G. Tosello, H. N. Hansen, Rheology of high melt strength polypropylene for additive manufacturing, Adv. Mater. Lett. 8 (2017) 712–716. doi:10.5185/amlett.2017.1450.
[28] D. Stoof, K. Pickering, 3D Printing of Natural Fibre Reinforced Recycled Polypropylene, in: Process. Fabr. Adv. Mater., The University of Auckland, 2017: pp. 668–691. http://researchcommons.waikato.ac.nz/handle/10289/11095.
[29] L. Wang, D.J. Gardner, Effect of fused layer modeling (FLM) processing parameters on impact strength of cellular polypropylene, Polymer (Guildf). 113 (2017) 74–80. doi:10.1016/j.polymer.2017.02.055.
[30] L. Wang, W. Gramlich, D. Gardner, Y. Han, M. Tajvidi, Spray-Dried Cellulose Nanofibril-Reinforced Polypropylene Composites for Extrusion-Based Additive Manufacturing: Nonisothermal Crystallization Kinetics and Thermal Expansion, J. Compos. Sci. 2 (2018) 7. doi:10.3390/jcs2010007.
[31] M. Katschnig, F. Arbeiter, B. Haar, G. van Campe, C. Holzer, Cranial Polypropylene Implants by Fused Filament Fabrication, Adv. Eng. Mater. 19 (2017) 1600676. doi:10.1002/adem.201600676.
[32] Q. Spiller, J. Fleischer, Additive manufacturing of metal components with the ARBURG plastic freeforming process, CIRP Ann. 67 (2018) 225–228. doi:10.1016/j.cirp.2018.04.104.
[33] ASTM Standard D1938-02, A.S. D1938-02, ASTM Standard D1938-02, Tear-Propagation Resistance of Plastic Film and Thin Sheeting by a Single-Tear Method, ASTM Int. West Conshohocken, PA. (2002) 5–8. doi:10.1520/D1922-15.2.
[34] M. Samykano, S.K. Selvamani, K. Kadirgama, W.K. Ngui, G. Kanagaraj, K. Sudhakar, Mechanical property of FFF printed ABS: influence of printing parameters, Int. J. Adv. Manuf. Technol. 102 (2019) 2779–2796. doi:10.1007/s00170-019-03313-0.
[35] R.J. Zaldivar, D.B. Witkin, T. McLouth, D.N. Patel, K. Schmitt, J.P. Nokes, Influence of processing and orientation print effects on the mechanical and thermal behavior of 3D-Printed ULTEM ® 9085 Material, Addit. Manuf. 13 (2017) 71–80. doi:10.1016/j.addma.2016.11.007.
[36] H.L. Tekinalp, V. Kunc, G.M. Velez-Garcia, C.E. Duty, L.J. Love, A.K. Naskar, C.A. Blue, S. Ozcan, Highly oriented carbon fiber–polymer composites via additive manufacturing, Compos. Sci. Technol. 105 (2014) 144–150. doi:10.1016/j.compscitech.2014.10.009.

Graphical Abstract